INORGANIC CHEMISTRY

FRONTIERS

Accepted Manuscript

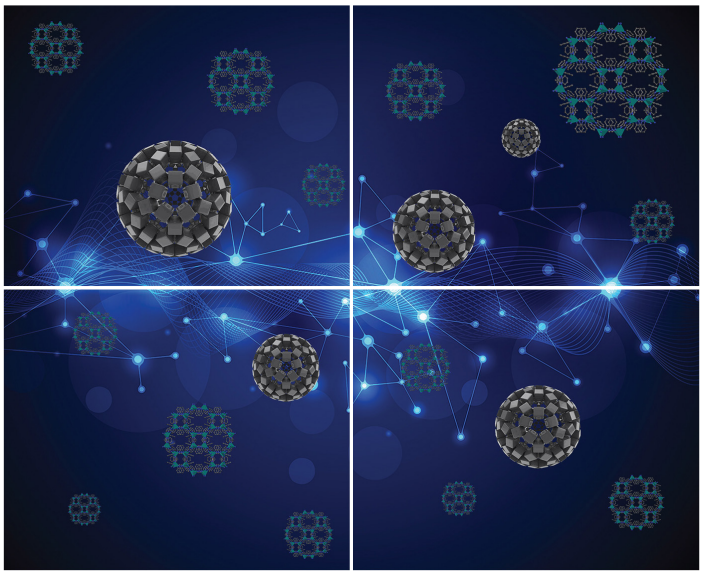

This article can be cited before page numbers have been issued, to do this please use: A. A. Mukhacheva, V. V. Yanshole, M. V. Il'in, A. S. Novikov, D. Bolotin, M. N. Sokolov and P. A. Abramov, *Inorg. Chem. Front.*, 2024, DOI: 10.1039/D4QI02258K.

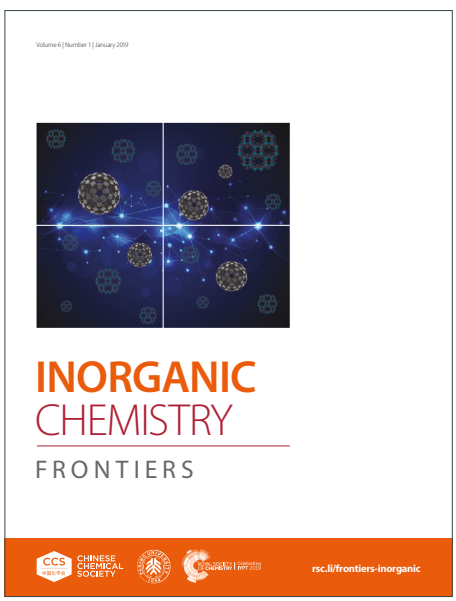

Chalcogen bond provided supramolecular association of beta-octamolybdate and chalconium cations

View Article Online
DOI: 10.1039/D4QI02258K

Anna A. Kuznetsova,[a] Vadim V. Yanshole,[b,c] Mikhail V. Il'in,[d] Alexander S. Novikov,[d,e] Dmitrii S. Bolotin,[d] Maxim N. Sokolov[a] and Pavel A. Abramov*[a,f]

[a] *Nikolaev Institute of Inorganic Chemistry, 3 Akad. Lavrentiev Ave. 630090, Russian Federation;*

[b] *International Tomography Center, Institutskaya str. 3a, 630090, Novosibirsk, Russian Federation;*

[c] *Novosibirsk State University, Pirogova str. 1, 630090, Novosibirsk, Russian Federation;*

[d] *Institute of Chemistry, Saint Petersburg State University, Universitetskiy prospect 26, Saint Petersburg, 198504, Russian Federation;*

[e] *Research Institute of Chemistry, Peoples' Friendship University of Russia (RUDN University), Miklukho-Maklaya Str. 6, 117198 Moscow, Russian Federation;*

[f] *Research School of Chemistry and Applied Biomedical Sciences, Tomsk Polytechnic University, Tomsk 634050, Russian Federation*

Abstract The interactions of triple σ-(Q^{IV})-hole donating chalconium cations ($[Q(bPh)R]^+$, when Q = S, Se, Te) with nucleophilic beta-octamolybdate ($[\beta\text{-}Mo_8O_{26}]^{4-}$) results in supramolecular association. The main focus of such assembling is on σ-(Q^{IV})-holes recognition by the molybdate in cations with a biphenyl aromatic fragment. This leads to a remarkable diversity of the association patterns producing: i) neutral 4:1 $\{[Q(bPh)R]_4[\beta\text{-}Mo_8O_{26}]\}$ complexes with cations stacked by π-π interactions; ii) $(Bu_4N)^+$, $[Q(bPh)R]^+$ and $[\beta\text{-}Mo_8O_{26}]^{4-}$ complexes of 2:2:1 stoichiometry with π-π interactions; iii) $(Bu_4N)^+$, $[Q(bPh)R]^+$ and $[\beta\text{-}Mo_8O_{26}]^{4-}$ complexes of 2:2:1 stoichiometry without π-π interactions; iv) $\{[Q(bPh)R]_2\}_2[\beta\text{-}Mo_8O_{26}]$ salts with π-π stacked cations but lacking any (Q^{IV})···O interactions. Moreover, interactions in the system can drive the reorganization of $[\beta\text{-}Mo_8O_{26}]^{4-}$ into $[\alpha\text{-}Mo_8O_{26}]^{4-}$. The halogen-bonded ($Q^{IV}$)···O $\{(Q(bPh)R)_x[\beta\text{-}Mo_8O_{26}]^{4-}\}$ (x = 2, 4) assemblies, π-π stacked cationic dimers $\{(Q(bPh)R)_2\}^{2+}$ and complicated associates based on both types interactions have been the subjects of crystallographic and computational studies.

Keywords: Chalcogen bonding; chalconium; octamolybdate; σ-hole; π-π stacking interactions

ORCIDS

View Article Online
DOI: 10.1039/D4QI02258K

Anna A. Kuznetsova 0000-0001-5648-8402

Vadim V. Yanshole 0000-0003-1512-3049

Mikhail V. Il'in 0000-0003-4234-4779

Alexander S. Novikov 0000-0001-9913-5324

Dmitrii S. Bolotin 0000-0002-9612-3050

Maxim N. Sokolov 0000-0001-9361-4594

Pavel A. Abramov 0000-0003-4479-5100

View Article Online
DOI: 10.1039/D4QI02258K

Introduction

Chalcogen- and halogen-containing organoelement species featuring a region with positive electrostatic potential on the heteroatom (σ-hole) have been extensively explored, since they effectively mimic the properties of metal-containing Lewis acids.[1] Such σ-hole donors demonstrate significant catalytic activity in the reactions requiring electrophilic activation of the substrates accompanied by notable tolerance to water and oxygen. The Lewis acidity of chalcogen (ChB)[2–4] and halogen (XB)[5–7] bond donors has similar trends, and it gradually rises from the lighter to heavier chalcogen or halogen σ-hole carriers, respectively.[8] Accordingly such compounds serve as electrophilic catalysts, tellurium- and iodine-based σ-hole donors exhibiting the highest catalytic activity, which is provided by ligation of the reaction substrates to the heteroatom σ-hole, leading to electrophilic activation of this substrate.

All the known σ-hole donors can be classified into several types. The first type substrates are represented by neutral organoelement compounds such as tetrabromomethane[9,10] or iodoperfluoroarenes.[5,11] The second type species are *cationic* organoelement compounds, which possess a significantly higher Lewis acidity. In particular, among the XB donors, iodopyridiniums[12,13] and iodoazoliums[14–17] featuring exocyclic iodine(I) atom effectively activate substrates via their ligation to the σ-hole in an extensive series of organic transformations, whereas among the ChB donors, the species featuring R_3Te^+ moiety show the most significant Lewis acidity.[18,19]

The third type σ-hole donors involve chalconium and halonium salts, which contain chalcogen(IV) or halogen(III). Iodonium salts possess a greater Lewis acidity than the iodine(I) derivatives,[20–26] whereas telluronium salts exhibit a significantly higher Lewis acidity than the neutral tellurium(II) derivatives or the sulfonium and selenonium cations.[19,27–35,36,37] Last, but not the least, neutral Te(IV) catecholates ($Te(cat)_2$) have remarkable Lewis acidity due to the presence of four σ-holes.[38,39]

This acidity can be used to create new supramolecular systems by exploiting high Lewis basicity of the O^{2-} ligands in the highly negatively charged polynuclear metal oxocomplexes known as polyoxometalates (POMs).[40] The chemistry of POMs in aqueous is complicated due to the pH induced equilibria and association with alkali cations (especially for group 5 complexes[41,42]) in water. In this regard, the use of non-aqueous solvents can produce impressive organic-inorganic hybrids, e.g. {Ag(SR)} / POM hydrids[43–47], POM-MOF materials,[48–52] etc.

In our ongoing research, we study the coordination chemistry of POMs as ligands in order to achieve new complexes with unusual structure and reactivity.[53–55] Such an approach utilizes vacant POMs (lacunary type) to induce coordination of heterometals under appropriate conditions. For example, in the studies of the coordination behavior of Ag^+ in different organic solvents, we used bis-

lacunary beta-octamolybdate ([β-Mo_8O_{26}]$^{4-}$, commonly accessible as *n*-Bu_4N^+ salt, Fig. 1) featuring various auxiliary ligands.[55] In these studies we discovered the ability of [β-Mo_8O_{26}]$^{4-}$ to interact with C-H, N-H or O-H groups[56], which is a key point in creating new supramolecular systems utilizing noncovalent interactions (NCIs). We have noticed that onium cations can serve as promising candidates for association with bis-lacunary beta-octamolybdate by the formation of σ-(X)-hole···O^{2-}=Mo bonding due to the presence of electronic pool on the oxoligands which define the two squares on the opposing sides of the anion. Iodonium cations are well-known building blocks for supramolecular association and crystal design.[57–65] Several recent reviews summarize iodonium cations reactivity.[66–70]

Recently we have found the iodonium cations (R_2I^+) "key-to-lock" recognition assembling by beta-octamolybdate via interactions between lacunary oxo-ligands and σ-(I^{3+})-holes. This supramolecular R_2I^+···O=Mo binding is based on two-center, three-center (bifurcated), and unconventional "orthogonal" I···O halogen bonds.[71] The later one is out of standard IUPAC criteria for the definition of the halogen bond due to the orthogonal location of the oxygen atom to the C–I–C plane of the interacting iodonium cation. Such an approach unlocks the potential of beta-octamolybdate for non-classical supramolecular coordination with σ-hole donors. Although this coordination superficially remands classical coordination of the cations like Na^+[72] or Ln^{3+},[73] the nature of the association is quite different.

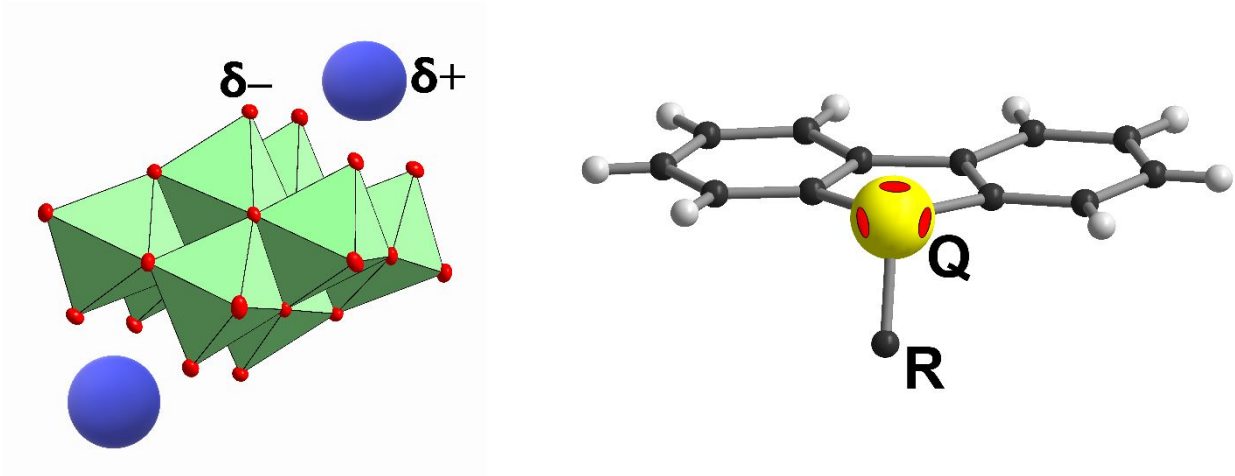

Figure 1. The structure of [β-Mo_8O_{26}]$^{4-}$ with highlighted nucleophilic O-flanked rims (left) and chalconium [Q(bPh)R]$^+$ cations with highlighted bPh ($C_{12}H_8$) fragment (right).

In this work, we introduce $[Q(bPh)R]^+$ chalconium cations (Q = S, Se, Te; R = Ph, 2,4,6-$(CH_3)_3C_6H_2$ = Mes, R = 4-BrC_6H_4, 4-FC_6H_4) (Figure 1, right) in the association with the $[\beta\text{-}Mo_8O_{26}]^{4-}$ platform. An important feature that determined our choice of the chalconium cations is that each cation has a biphenil bPh ($C_{12}H_8$) liable to participate in π-π interactions. This feature opens different pathways for the organization of chalconium cations and $[\beta\text{-}Mo_8O_{26}]^{4-}$ anions in the crystal, which follow at least three different patterns: i) classical π-π stacking cancels cation-to-anion binding; ii) non-classical σ-(Q^{IV})-hole···O=Mo (ChB) interactions cancel staking; iii) both types of interactions materialize. It is expected that the nature of chalcogen would affect the strength of ChB interactions and the pattern of supramolecular association.

Results and discussion

Synthesis and characterization

We selected the set of chalconium triflates [Q(bPh)R](OTf) (Q = S, Se, Te; bPh = $C_{12}H_8$; R = Ph, 2,4,6-$(CH_3)_3C_6H_2$, 4-BrC_6H_4, 4-FC_6H_4; $OTf^- = CF_3SO_3^-$) for the cation exchange reactions with $(n\text{-}Bu_4N)_4[\beta\text{-}Mo_8O_{26}]$. The synthetic procedures were done in different solvents (DMF, DMSO, NMP) at 4:1 cation:anion stoichiometry at room temperature. The products typically precipitated (amorphous or crystalline) within a few minutes after the mixing of the reagents. When direct precipitation did not work, conventional vapor diffusion was used for crystallization, with: i) Et_2O in the case of DMF or NMP solutions and ii) *i*-PrOH or hexane in the case of DMSO solutions. In total we isolated and characterized by SCXRD 9 new chalconium salts of $[\beta\text{-}Mo_8O_{26}]^{4-}$ (see Table 1). All the data regarding synthesis and characterization are summarized in Supporting information.

According to the literature, $[\beta\text{-}Mo_8O_{26}]^{4-}$ is not a single form in the solution and commonly equilibrates with $[\alpha\text{-}Mo_8O_{26}]^{4-}$ and $[Mo_6O_{19}]^{2-}$.[56,72] The latter appears in the presence of water or traces of H^+. The equilibrium between $[\beta\text{-}Mo_8O_{26}]^{4-}$ and $[\alpha\text{-}Mo_8O_{26}]^{4-}$ slowly gives the α-isomer as major species, but it can be reversed by electrophiles stabilizing $[\beta\text{-}Mo_8O_{26}]^{4-}$ form by coordination. In our case, we isolated $[S(bPh)Ph]_4[\alpha\text{-}Mo_8O_{26}]\cdot 2DMSO$ (**2**) and $(Bu_4N)_2[S(bPh)Mes]_2[\alpha\text{-}Mo_8O_{26}]\cdot 2DMF$ (**3**) containing α-isomer of octamolybdate. This indicates that equilibria between different POMs can be shifted by the thermodynamically favorable crystalline phase formation.

Also noteworthy is the formation of 4:1 ($[Q(bPh)R]_4[\beta\text{-}Mo_8O_{26}]$) and 2:2:1 ($(Bu_4N)_2[Q(bPh)R]_2[\beta\text{-}Mo_8O_{26}]$) cation/anion combinations in the above-mentioned synthetic procedures. This outcome is not predictable and evades simple explanation. Thus we observed the formation of the fully substituted 4:1 salts in the case of $[S(bPh)Ph]_4[\beta\text{-}Mo_8O_{26}]$ (**1**), $[S(bPh)Mes]_4[\beta\text{-}Mo_8O_{26}]\cdot 2DMF\cdot 0.6H_2O$ (**4**) and $[Te(bPh)Ph]_4[\beta\text{-}Mo_8O_{26}]\cdot 2MeOH$ (**[9]·2CH$_3$OH**).

Table 1. Complexes studied in this work

Complex	Chalconium cation	Composition
1	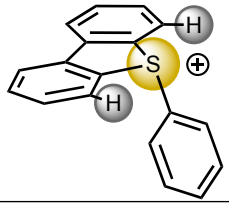	$[S(bPh)Ph]_4[\beta\text{-}Mo_8O_{26}]$
2		$[S(bPh)Ph]_4[\alpha\text{-}Mo_8O_{26}]\cdot 2DMSO$
3	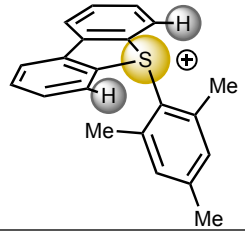	$(Bu_4N)_2[S(bPh)Mes]_2[\alpha\text{-}Mo_8O_{26}]\cdot 2DMF$
4		$[S(bPh)Mes]_4[\beta\text{-}Mo_8O_{26}]\cdot 2DMF\cdot 0.6H_2O$
5	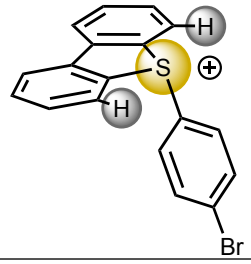	$(Bu_4N)_2[S(bPh)C_6H_4Br]_2[\beta\text{-}Mo_8O_{26}]\cdot 2DMF$
6	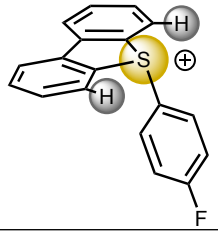	$(Bu_4N)_2[S(bPh)C_6H_4F]_2[\beta\text{-}Mo_8O_{26}]\cdot 2DMF$
7	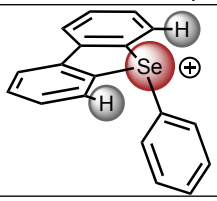	$(Bu_4N)_2[Se(bPh)Ph]_2[\beta\text{-}Mo_8O_{26}]$
8	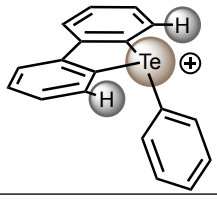	$(Bu_4N)_2[Te(bPh)Ph]_2[\beta\text{-}Mo_8O_{26}]$
([9]·2CH$_3$OH		$[Te(bPh)Ph]_4[\beta\text{-}Mo_8O_{26}]\cdot 2MeOH$

On the other side, the 2:2:1 salts were found for $(Bu_4N)_2[S(bPh)Mes]_2[\alpha\text{-}Mo_8O_{26}]\cdot 2DMF$ (**3**), $(Bu_4N)_2[S(bPh)C_6H_4Br]_2[\beta\text{-}Mo_8O_{26}]\cdot 2DMF$ (**5**), $(Bu_4N)_2[S(bPh)C_6H_4F]_2[\beta\text{-}Mo_8O_{26}]\cdot 2DMF$ (**6**), $(Bu_4N)_2[Se(bPh)Ph]_2[\beta\text{-}Mo_8O_{26}]$ (**7**), and $(Bu_4N)_2[Te(bPh)Ph]_2[\beta\text{-}Mo_8O_{26}]$ (**8**). Such a division was also found for iodonium salts of $[\beta\text{-}Mo_8O_{26}]$.[71] This bifurcation in the reaction outcome looks like a general feature which can be caused by an interplay of noncovalent interactions (NCIs) like C-H···O=Mo, π-π and ChB bonding in the solid state.

In this work we detected several modes of interplay between ChB and π-π interactions: i) domination of classical π-π stacking without cation-to-anion binding (for complexes **3**, **4**); ii)

domination of non-classical σ-(Q^{IV})-hole···O=Mo (ChB) interactions without stacking interactions (complexes **7**, **8**); iii) more complicated association including both types of interactions (complexes **1**, **2**, **5**, **6**, **[9]·2CH$_3$OH**). Two different types of π-π stacked dimers of $[S(bPh)Mes]^+$ cations (see Fig. S4, S5 in SI) have been observed. In both cases (**3** and **4**), σ-(Q^{IV})-hole···O=Mo (ChB) interactions are blocked, and cations and anions reveal only C-H···O=Mo contacts.

The lion's share of the presented structures contains several types of interactions that complement each other (complexes **1**, **2**, **5**, **6**, **[9]·2CH$_3$OH**). The "exceptions from the rules" for **3** and **4** are likely caused by the specific nature of $[S(bPh)Mes]^+$ which has (i) steric hindrance due to the presence of three methyl groups and (ii) strongest electron donation from the Mes substituent. The strength of non-classical σ-(Q^{IV})-hole···O=Mo (ChB) interactions in the crystal structures of **7** and **8** can block stacking between the cations, which is also disrupted by the presence of Bu_4N^+ cations. This effect illustrates preference of combined ChB and C-H···O=Mo contacts over π-π interactions. The arrangement of anion and cations linked by ChB in **7** and **8** is different in comparison with **1**–**6** due to the change in chalcogen type. This will be discussed later in the NCI analysis section.

To prove the existence of σ-(Q^{IV})-hole···O=Mo interactions in complex solutions is a challenging task. In our experiments ^{1}H NMR spectra showed absence of any significant change in the chalconium cation protons chemical shifts in the presence of β-$Mo_8O_{26}]^{4-}$. The mass-spectrometry (HR-ESI-MS) characterization of complex solutions did reveal the presence of ionic peaks from {x$[Q(bPh)R]^+$ + [β-$Mo_8O_{26}]^{4-}$} associates. The example of such spectrum is presented in SI for complex **1** in CH_3CN solution (see Fig. S6-S10 and Table S2 in SI). This observation might indicate an association in solution between chalconium cations and beta-octamolybdate.

NCI analysis

1. Sulfonium cation as a ChB donor

The analysis of noncovalent interactions (NCIs) is commonly based on the Van der Waals radii of interacting atoms. In our case, we used the following values: R_{VdW}(O) 1.52 Å, R_{VdW}(S) 1.80 Å, R_{VdW}(Se) 1.90 Å, R_{VdW}(Te) 2.00 Å.[74] The largest respective interatomic distances are 3.32, 3.42, and 3.80 Å. We also illustrated positions of σ-holes (σ-(Q^{IV})-hole) over the surface of the chalcogen atom in $[Q(bPh)R]^+$ chalconium cations. According to the definition, each Q-atom has three σ-holes located opposite to the three Q-C bonds (Fig. 1 right). Such an arrangement of the σ-holes leads to the trigonal pyramidal geometry of binding with the donors of electronic density. β-Octamolybdate has two lacunae each flanked with four terminal O^{2-} ligands (Fig. 1). The arrangement of these oxoligands favors square-pyramidal coordination of the Lewis acidic center, and thus the interaction should require adaption between donor and acceptor geometries.

In the case of sulfonium cations and beta-octamolybdate structures reported here, we found two binding modes between cations and anion involving σ-(S^{IV})-hole···O=Mo interactions (Fig. 2), which were analyzed in terms of NCIs (Table 2).

Table 2. Geometric parameters of NCIs with the lacuna rims in the structures of **1, 2, 5** and **6.**

Complex	d(S···O), Å / *N*c[a]	∠(C-S···O) °	NCI type
1a	d(S1···O2) = 2.935(3) / 0.88	C12–S1···O2 = 161.83	ChB
	d(S1···O6) = 2.731(2) / 0.82	C1-S1···O6 = 162.96	ChB
	d(S2···O1) = 2.912(3) / 0.88	C48-S2···O1 = 164.19	ChB
	d(S2···O10) = 2.875(2) / 0.86	C37-S2···O10 = 156.26	ChB
	d(S2···O11) = 3.102(3) / 0.93	C48-S2···O11 = 111.75	ICS
1b	d(S3···O15) = 2.964(3) / 0.89	C26-S3···O15 = 156.79	ChB
	d(S3···O17) = 2.757(2) / 0.83	C19-S3···O17 = 166.22	ChB
	d(S4···O14) = 2.856(2) / 0.86	C66-S4···O14 = 162.39	ChB
	d(S4···O21) = 2.801(2) / 0.84	C55-S4···O21 = 156.39	ChB
2	d(S1···O5) = 3.296(3) / 0.99	C1-S1···O5 = 154.50	ChB
	d(S1···O8) = 2.901(3) / 0.87	C13-S1···O8 = 164.68	ChB
5	d(S1···O8) = 2.747(2) / 0.83	C1-S1···O8 = 166.26	ChB
	d(S1···O10) = 2.766(2) / 0.83	C12-S1···O10 = 168.66	ChB
6	d(S1···O3) = 2.755(2) / 0.83	C6-S1···O8 = 168.94	ChB
	d(S1···O5) = 2.765(2) / 0.83	C12-S1···O5 = 164.42	ChB

[a]The normalized contact (Nc) is defined as the ratio between the separation observed in the crystal and the sum of Bondi vdW radii of interacting atoms: *N*c = *d*/ΣvdW; ΣvdW S + O = 3.32 Å. ICS = induced short contact.

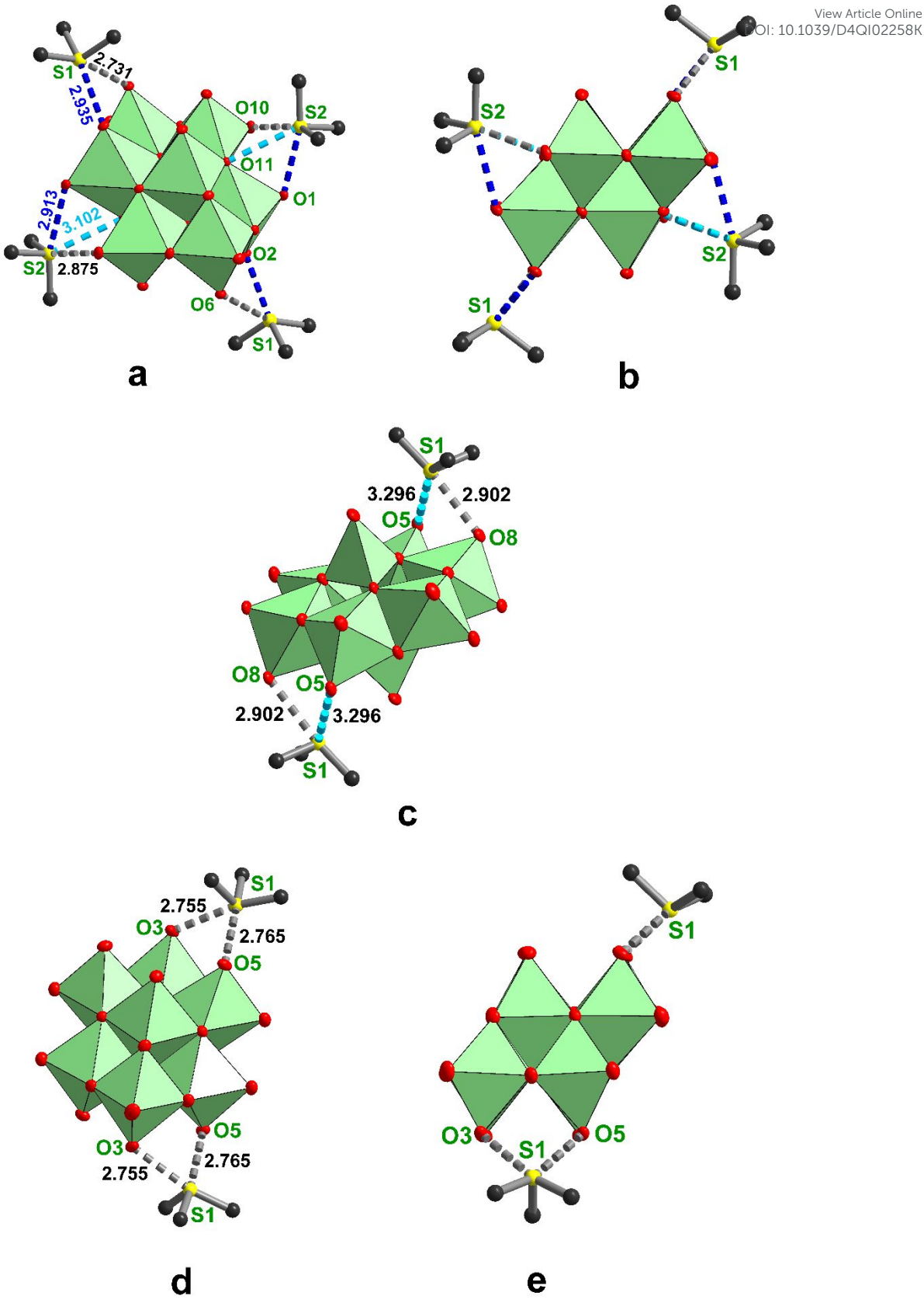

Figure 2. σ-(S^{IV})-hole···O=Mo interactions in the crystal structures of **1a** (a, b), **2**(c), **6**(d, e). Contacts: between 2.7–2.9 Å are grey, between 2.9–3.0 Å are blue and over 3.0 Å are cyan.

The first binding mode is based on the formation of one strong σ-(S^{IV})-hole···O=Mo contact with *N*c from 0.82 (for **1a**) to 0.87 (for **2**) accompanied by one or two weaker contacts. The second mode utilizes two strong σ-(S^{IV})-hole···O=Mo contacts with *N*c 0.83 (for **5** and **6**).

In terms of IUPAC criteria,[75] the C-S···O contacts can be two-center ChB or bifurcated ChB. The corresponding angles can vary in 160–180° and 135–160° range. The bifurcated bonds have longer S···O distances than the two-center ChB. It should be noted that there is one S···O contact (**1a**, S2···O11) which cannot be associated with normal ChB according to the above-mentioned criteria, due to the significant deviation of C–S···O angle (111°) from linearity (Table 2). This can be assigned in two ways: i) induced short contact (ISC); ii) an unconventional ChB which can be defined as *orthogonal* ChB (oChB), probably of π-hole nature. See details in the calculation part.

In the crystal structure of **1**, two crystallographically independent $\{[S(bPh)Ph]_4[Mo_8O_{26}]\}$ associates (named as **1a** and **1b**) are observed, which differ in the mode of cation-anion binding. The main difference is the absence of ISC (for **1b**) contact between S4 and O, which is observed in **1a** (see Table 1). Both $\{[S(bPh)Ph]_4[Mo_8O_{26}]\}$ associates have an inversion center located in the center of gravity of beta-octamolybdate. To simplify the further description, we highlighted the $\{[S(bPh)Ph]_2[Mo_8O_{26}]\}^{2-}$ unit only with the cations coordinated to the O-flanked rims of POM. We notate this unit as *sym*-$\{[S(bPh)R]_2[Mo_8O_{26}]\}^{2-}$ to specify this type of binding.

In the crystal structure of isostructural **5** and **6**, changes in the cation-to-anion binding distort the symmetry of supramolecular associate, which loses the inversion center (Fig. 2d. 2e). In these structures, we deal with the *asym*-$\{[S(bPh)R]_2[Mo_8O_{26}]\}^{2-}$ unit when the sulfur atoms of two coordinated cations and the center of gravity of the beta-octamolybdate are not coplanar. The visual difference between *sym*-$\{[S(bPh)R]_2[Mo_8O_{26}]\}^{2-}$ and *asym*-$\{[S(bPh)R]_2[Mo_8O_{26}]\}^{2-}$ is seen in Fig. 2b and Fig. 2e. Crystal structures of the previously reported associates with iodonium cations demonstrate the formation of only *sym*-$\{[IR_2]_2[Mo_8O_{26}]\}^{2-}$ supramolecular associates.[71]

The reported sulfonium salts of POMs are all different in terms of NCIs. In the case of $(CPDS)_4[Mo_8O_{26}]$ (CPDS = 4-chlorophenyl(dimethyl)sulfonium, CCDC 2109715, YAWREX), the sulfonium cations are not bonded to beta-octamolybdate at all, being linked only to H_2O (d(S···O) = 2.941(3) Å) and Cl (d(S···Cl) = 3.648(3) Å).[76] In $(HPDS)_4[Mo_8O_{26}]$ (HPDS = (4-hydroxyphenyl)dimethylsulfonium, CCDC 1536033, LEHDIO), there is a S···μ_2-O contact of 3.229(3) Å.[77] The structure of $(MAPDS)_4[Mo_8O_{26}]$ (MAPDS = 4-(methacryloyloxy)phenyl)-dimethylsulfonium, CCDC 1536038, LEHFIQ) shows an interaction of σ-(S^{IV})-hole···O=Mo type of 3.183(3) Å. However, beta-octamolybdate salts with (4-hydroxy-2-methylphenyl)dimethylsulfonium, (4-methoxyphenyl)dimethylsulfonium, (4-(allyloxy)phenyl)dimethylsulfonium and 4-(allyloxy)-2-methylphenyl)dimethylsulfonium do not show any σ-(S^{IV})-hole···O=Mo interactions.[77] These salts were obtained by the treatment of the

sulfonium triflate (1.5 equiv.) with sodium molybdate (1 equiv.) in water at pH 4.0. It seems that both crystallization from aqueous solution and specific nature of organic substituents at sulfur hinder the formation of proper σ-(S^{IV})-hole···O=Mo bonding interactions.

The oldest known sulfonium salt of beta-octamolybdate is trimethylsulfonium salt $(Me_3S)_4[Mo_8O_{26}]$ (CCDC 907956, DEPNUM) reported by Mialane et al.[78] obtained from an acidified aqueous solution of Na_2MoO_4 (3 mmol) and $(Me_3S)(NO_3)$ (3 mmol). In the crystal structure, $[Mo_8O_{26}]^{4-}$ has 8 σ-(S^{IV})-hole···O=Mo contacts (eight contacts due to positional disorder of the cations) ranging between 2.770(3) and 3.203(4) Å. Each cation generates only one contact with the anion. The lack of involvement of other σ-holes to form second and third ChB may be a result of electron donating nature of CH_3 which lowers the Lewis acidity of the chalcogen. The lacunary oxoligands participate in the formation of the strongest ChB at 2.770(3) and 2.905(4) Å with Me_3S^+ located as in *sym*-$\{[S(bPh)Ph]_2[Mo_8O_{26}]\}^{2-}$ (Fig. S11).

2. Q = Se

The crystal structure of $(Bu_4N)_2[Se(bPh)Ph]_2[\beta\text{-}Mo_8O_{26}]$ (**7**) demonstrates the general structural feature resulting from the change of S to Se in the same type $[Q(bPh)Ph]^+$ cation. Two lacunae of beta-octamolybdate catch the selenium atoms (Fig. 3) generating four σ-(Se^{IV})-hole···O=Mo NCIs for each interacting selenonium cation (Table 3).

Table 3. Geometric parameters of σ-(Se^{IV})-hole···O=Mo NCIs in the structure of **7**.

Complex	d(Se···O), Å / *Nc*[a]	∠(C-Se···O)	NCI type
7	d(Se1···O10) = 2.755(2) / 0.81	C13-Se1···O10 = 171.58	ChB
	d(Se1···O3) = 2.935(3) / 0.86	C12-Se1···O3 = 157.51	ChB
	d(Se1···O1) = 3.306(3) / 0.97	C12-Se1···O1 = 127.94	ICS
	d(Se1···O12) = 2.912(3) / 0.85	C1-Se1···O12 = 143.79	ChB
	d(Se1···O1) = 3.306(3) / 0.97	C1-Se1···O1 = 145.17	ISC

[a]The normalized contact (Nc) is defined as the ratio between the separation observed in the crystal and the sum of Bondi vdW radii of interacting atoms: Nc = *d*/ΣvdW; ΣvdW Se + O = 3.42 Å. ISC = induced short contact.

The strongest ChB has d(Se1···O10) = 2.755(2) Å and can be classified as normal two-center ChB, whereas two other contacts can be assigned as a combination of ChB and ISC (in the case of *Nc* = 0.97). The only selenonium salt of beta-octamolybdate reported to date is $(MDPSe)_4[Mo_8O_{26}]$ (MDPSe = methyldiphenylselenonium) whose crystal structure is unknown.[79] It may involve σ-(Q^{IV})-hole···O=Mo bonding.

View Article Online
DOI: 10.1039/D4QI02258K

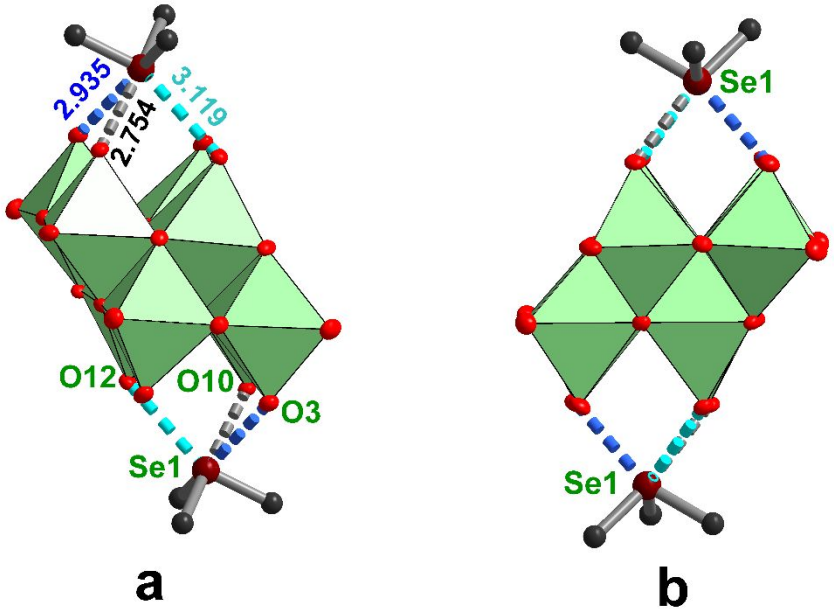

Figure 3. σ-(Se^{IV})-hole···O=Mo interactions in the crystal structure of **7**. Contacts: between 2.7–2.9 Å are grey, between 2.9–3.0 Å are blue and over 3.0 Å are cyan.

3. Q = Te

The behavior of $[Te(bPh)Ph]^+$ telluronium beta-octamolybdate is closer to its Se analogue. We isolated and structurally characterized both 2:2:1 and 4:1 salts as $(Bu_4N)_2[Te(bPh)Ph]_2[\beta\text{-}Mo_8O_{26}]$ (**8**) and $[Te(bPh)Ph]_4[\beta\text{-}Mo_8O_{26}]\cdot 2MeOH$ (**[9]·2CH$_3$OH**), respectively. The metrics of the corresponding NCIs are listed in Table 4. The representation of the corresponding *sym*-$\{[Te(bPh)Ph]_2[Mo_8O_{26}]\}^{2-}$ associate structures is shown in Figure 4.

Table 4. Geometric parameters of σ-(Te^{IV})-hole···O=Mo NCIs in the structures of **8** and **9**.

Complex	d(Te···O), Å / *Nc*[a]	∠(C-Te···O)	NCI type
8	d(Te1···O6) = 2.743(2) / 0.72	C1-Te1···O6 = 176.86	ChB
	d(Te1···O1) = 2.926(3) / 0.77	C18-Te1···O1 = 151.98	bChB
	d(Te1···O13) = 3.195(3) / 0.84	C18-Te1···O13 = 133.98	
	d(Te1···O11) = 3.000(3) / 0.79	C1-Te1···O11 = 144.25	bChB
	d(Te1···O13) = 3.195(3) / 0.84	C7-Te1···O13 = 144.55	
[9]·2CH$_3$OH	d(Te1···O1) = 2.912(3) / 0.77	C18-Te1···O1 = 178.53	ChB

	d(Te1···O4) = 3.028(3) / 0.80	C7-Te1···O4 = 160.50	ChB
	d(Te1···O9) = 3.070(3) / 0.81	C1-Te1···O9 = 141.75	bChB
	d(Te1···O12) = 3.241(3) / 0.85	C1-Te1···O12 = 145.10	
	d(Te2···O13) = 2.900(3) / 0.76	C37-Te2···O13 = 169.67	ChB
	d(Te2···O2) = 3.435(3) / 0.90	C20-Te2···O2 = 125.71	ISC
	d(Te2···O14) = 3.047(3) / 0.80	C26-Te2···O14 = 167.52	ChB

View Article Online
DOI: 10.1039/D4QI02258K

[a]The normalized contact (Nc) is defined as the ratio between the separation observed in the crystal and the sum of Bondi vdW radii of interacting atoms: Nc = *d*/ΣvdW; ΣvdW Te + O = 3.8 Å. ICS = induced short contact.

$[Te(bPh)Ph]^+$ cations interact with $[\beta\text{-}Mo_8O_{26}]^{4-}$ anion in different modes in the solid state. In the case of **8**, Te atom forms one strong two-center ChB (d(Te1···O6) = 2.743(2) Å) and two bifurcated ChBs with oxoligands at longer distances, stabilizing the supramolecular associate of the *sym*-$\{[Q(bPh)Ph]_2[Mo_8O_{26}]\}^{2-}$ type. Each Te atom is located above the center of the lacuna as defined by the plane of square of four terminal oxo ligands. In this case, the bonding distance criterion differentiates well between two-center and bifurcated ChB.

In the case of **[9]·2CH$_3$OH**, there are two types of $[Te(bPh)Ph]^+$ cations binding with $[\beta\text{-}Mo_8O_{26}]^{4-}$ anion via σ-(Te^{IV})-hole···O=Mo NCIs. Telluronium cations of the first type interact directly with two lacunae generating four ChBs between oxoligands and each Te atom. There are two two-center ChBs (d(Te1···O1) = 2.912(3) and d(Te1···O4) = 3.028(3) Å) and one bifurcated ChB (d(Te1···O9) = 3.070(3) and d(Te1···O12) = 3.241(3) Å). It should be noted that the length differentiation criterion for two-center and bifurcated ChB is unsatisfactory in this case. The comparison of NCIs in **8** and **[9]·2CH$_3$OH** indicates switching from one two-center ChB and two bChB in **8** for two two-center ChB and one bChB in the case of **[9]·2CH$_3$OH**. The reason for this can be formation of another NCIs in the crystal packing affecting organic groups of telluronium cations. Crystal structure of **8** have no π-π stacking interactions between $[Te(bPh)Ph]^+$ cations, whereas **[9]·2CH$_3$OH** forms plenty of such type interactions.

Telluronium cations of the second type are attached to *sym*-$\{[Te(bPh)Ph]_2[Mo_8O_{26}]\}^{2-}$ associate by one two-center ChB with terminal O=Mo (d(Te2···O13) = 2.900(3) Å) and one two-center ChB with O-atom of solvated CH_3OH (d(Te2···O14) = 3.047(3) Å). In addition, a weak contact with μ_2-O oxoligand of beta-octamolybdate (d(Te2···O2) = 3.435(3) Å) of oChB nature, according to the angle size criterion, is observed. Incorporation of CH_3OH molecules in the crystal structure might be a result of strong σ-(Te^{IV})-hole···O interactions.

Other telluronium salts of polyoxometalates are unknown. Kortz et al. reported two complexes $[(C_4H_8Te^{IV})_3(X^{III}W_9O_{33})_2]^{12-}$ (C_4H_8 = cyclobutyl, X = As, Sb) obtained from the reaction of $(C_4H_8)TeI_2$ with the trilacunary Keggin ions $[\alpha\text{-}X^{III}W_9O_{33}]^{9-}$ in water (pH 7.5).[76] The Te–O bond distances fill 2.063(15)–2.1309(15) Å interval, which is comparable with normal Te–O bonding in diaryltellurium oxide $[(p\text{-}MeOC_6H_4)_2TeO]_n$ (2.025(2) and 2.100(2) Å).[80]

View Article Online
DOI: 10.1039/D4QI02258K

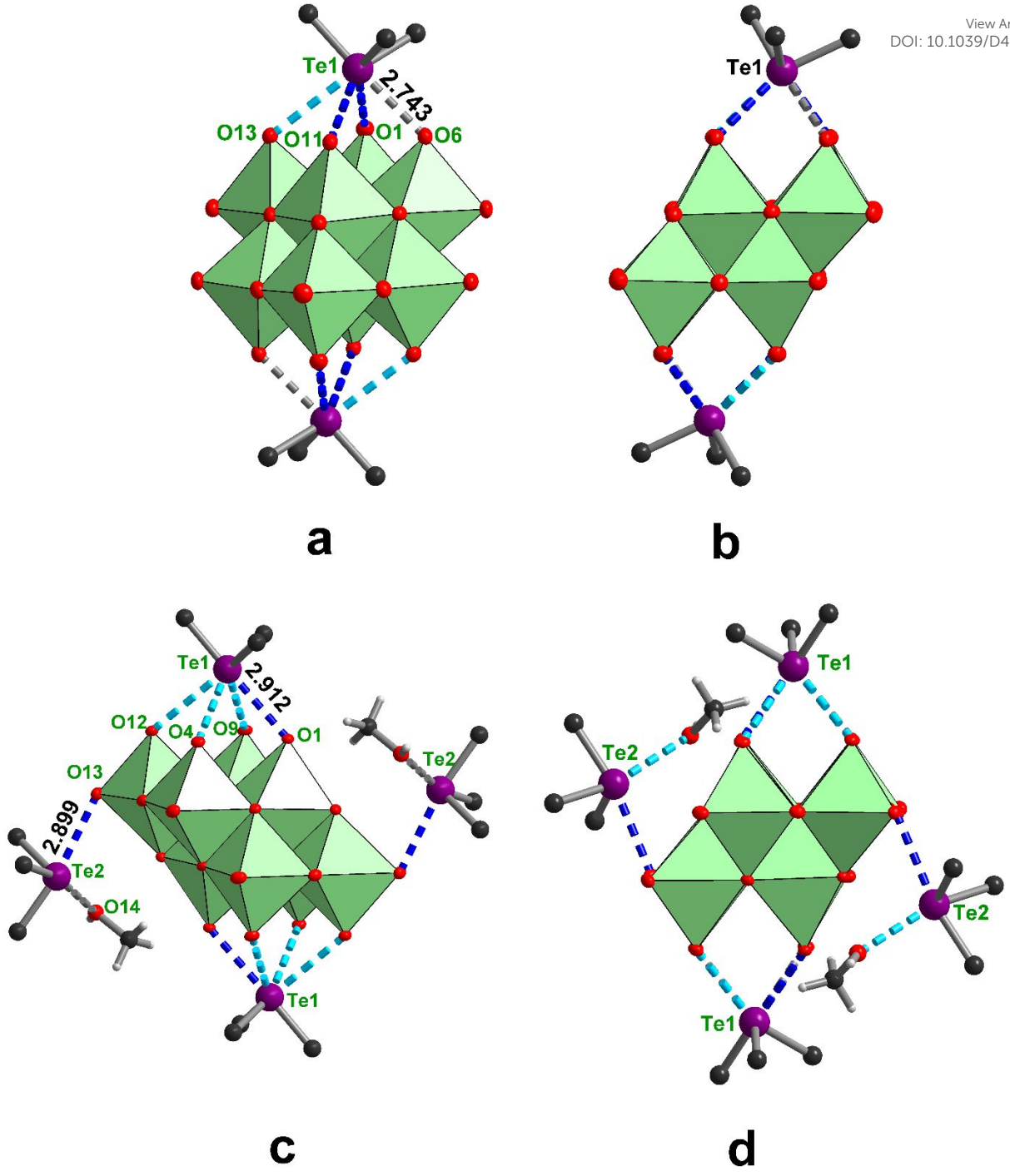

Figure 4. σ-(Te^{IV})-hole···O interactions in the crystal structures of **8** (a, b), **[9]·2CH$_3$OH** (c, d). Contacts: between 2.7–2.9 Å are grey, between 2.9–3.0 Å are blue and over 3.0 Å are cyan.

Comparison of onium adducts with beta-octamolybdate

To compare the NCIs generating by beta-octamolybdate and different σ-hole donors in $\{[X]_2[Mo_8O_{26}]\}^{2-}$ associates, we introduced angle size criterion associated with O…O…X angle (Fig. 5) defined as Δ. The experimental values are: Δ = 50.183(1)° for complex **1** (Q = S), Δ = 44.988(1)° for complex **6** (Q = S), Δ = 82.977(1)° for complex **7** (Q = Se), Δ = 90.558(1)° for complex **9** (Q = Te). In the case of $(Ph_2I)_4[\beta\text{-}Mo_8O_{26}]$ Δ is 81.143(1)°, whereas in $(Me_3S)_4[Mo_8O_{26}]$[78] the cations are linked with the anion in different modes (Fig. S11) and we cannot apply this criterion. It seems that aryl substituents are required at chalcogen to form *sym*-$\{[SR_3]_2[Mo_8O_{26}]\}^{2-}$ associate with a small Δ value.

Taking these data into account we can deduce some correlations in σ-hole acceptor and beta-octamolybdate arrangement: i) the increase in X-atom radius increases of O…O…X angle; ii) the increase in X-atom radius changes the bonding type between cation and beta-octamolybdate. To analyze the presented NCIs and π-π interactions in details we used quantum-chemical calculations described below.

View Article Online
DOI: 10.1039/D4QI02258K

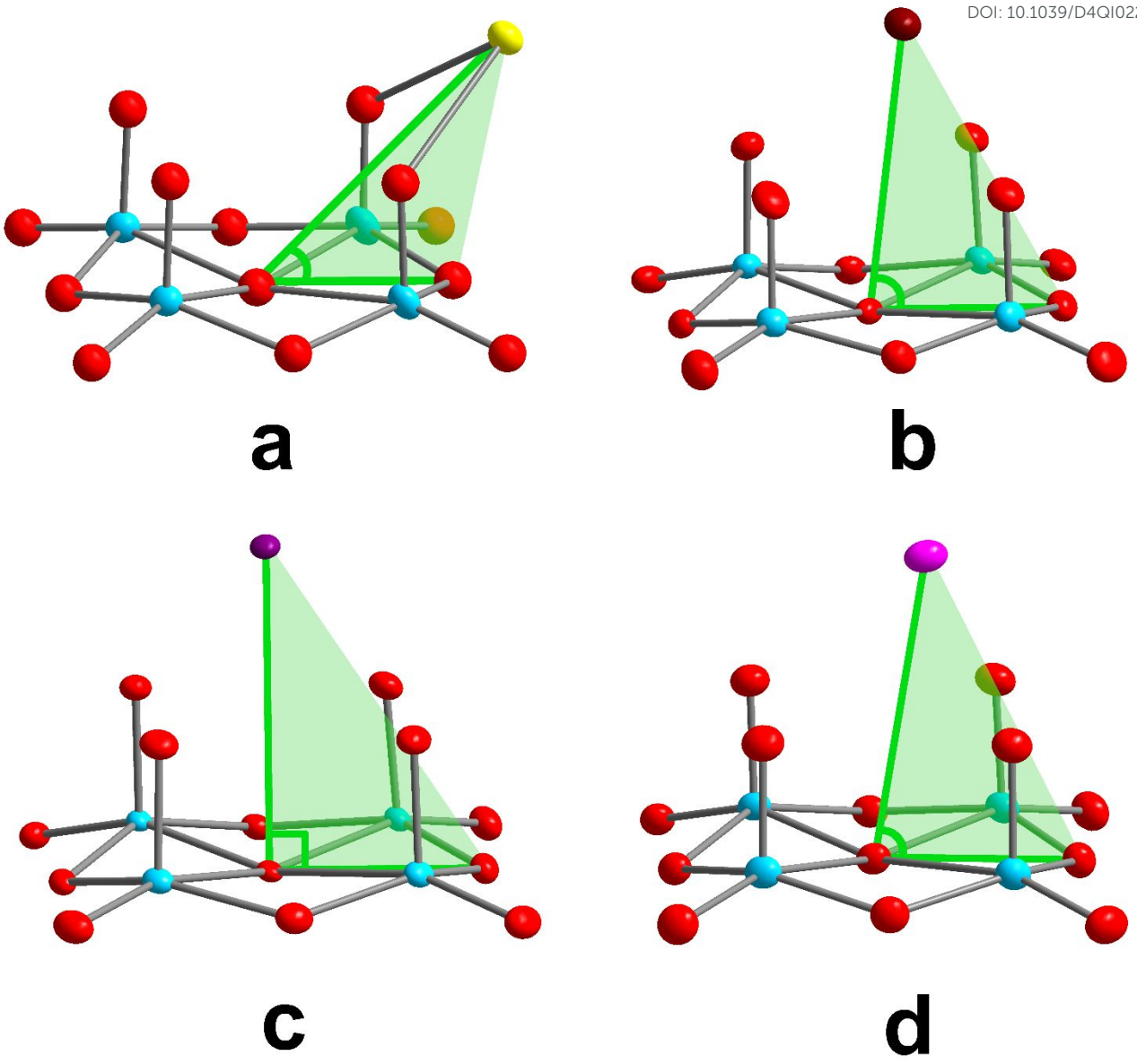

Figure 5. σ-(X)-hole···O=Mo interactions in the crystal structures of $[\beta\text{-}Mo_8O_{26}]^{4-}$ with some onium cations: complex **1** (a), complex **7** (b), complex **9** (c), $(Ph_2I)_4[\beta\text{-}Mo_8O_{26}]$ (d).

Calculations

To understand the nature and quantify the strength of intermolecular interactions Q···O (Q = S, Se, Te) in the structures **1**, **2, 5–[9]·2CH$_3$OH**, the DFT calculations followed by the topological analysis of the electron density distribution within the QTAIM approach[81] were carried out at the ωB97XD/DZP-DKH level of theory for model supramolecular associates (see Computational details and Table S3 in Supporting Information). Results of QTAIM analysis are summarized in Table S3, the contour line diagram of the Laplacian of electron density distribution $\nabla^2\rho(\mathbf{r})$, bond paths, and selected zero-flux surfaces, visualization of electron localization function (ELF) and reduced density gradient (RDG) analyses for intermolecular interactions S···O in the X-ray structure **6** shown in Figure 6. Bond critical points (3, –1) are shown in blue, ring critical points (3, +1) – in orange, nuclear critical points (3, –3) – in pale brown, cage critical points (3, +3) – in light green, bond paths are shown as pale brown lines, length units – Å, and the color scale for the ELF and RDG maps is presented in a.u.

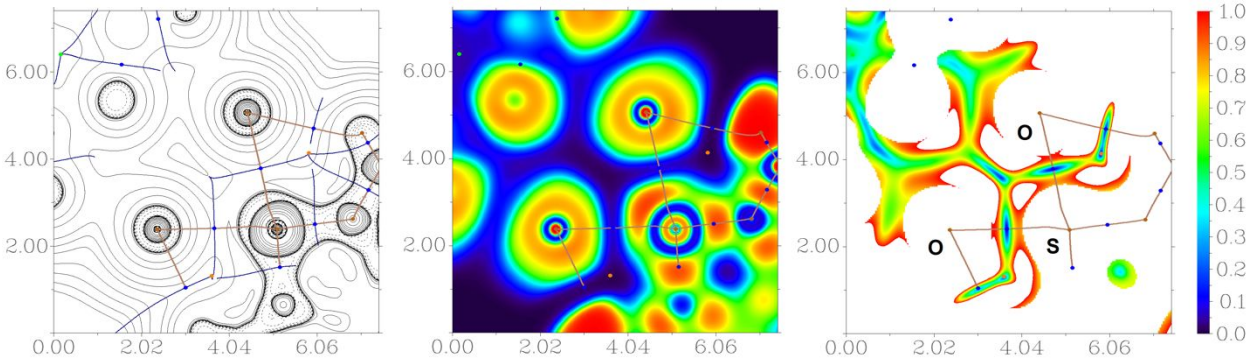

Figure 6. Contour line diagram of the Laplacian of electron density distribution $\nabla^2\rho(\mathbf{r})$, bond paths, and selected zero-flux surfaces (left panel), visualization of electron localization function (ELF, center panel) and reduced density gradient (RDG, right panel) analyses for intermolecular interactions S···O in the X-ray structure **6**.

The QTAIM analysis of model supramolecular associates demonstrates the presence of bond critical points (3, –1) for different intermolecular σ-(Q^{IV})-hole···O=Mo (Q = S, Se, Te) interactions in the structures of **1**, **2, 5–[9]·2CH$_3$OH** (Table S3). The low magnitude of the electron density (0.003–0.027 a.u.), positive values of the Laplacian of electron density (0.011–0.073 a.u.), and zero or very close to zero energy density (0.000–0.003 a.u.) in these bond critical points (3, –1), and estimated strength for appropriate short contacts (0.6–6.3 kcal/mol) are typical for noncovalent interactions in similar chemical systems.[55,82–85] Note that the balance between the potential and kinetic energy densities of electrons at the bond critical points (3, –1) for studied contacts reveals that these

interactions are purely noncovalent.[86] The Laplacian of electron density is typically decomposed into the sum of contributions along the three principal axes of maximal variation, giving the three eigenvalues of the Hessian matrix (λ_1, λ_2 and λ_3), and the sign of λ_2 can be utilized to distinguish bonding (attractive, $\lambda_2 < 0$) weak interactions from non-bonding ones (repulsive, $\lambda_2 > 0$).[87,88] Thus, the intermolecular σ-(Q^{IV})-hole···O=Mo (Q = S, Se, Te) interactions in **1**, **2, 5**–**[9]·2CH$_3$OH** are all attractive (Table S3).

The most challenging interactions are shown in Fig. 7. Calculated energies are: 2.2 kcal/mol for **1** (S2···O11); 1.3 kcal/mol for **7** (Se1···O1); 2.5 kcal/mol for **8** (Te1···O13) and 1.6 kcal/mol for **[9]·2CH$_3$OH** (Te2···O2). These interactions can be assigned in two ways: i) induced short contact (ISC); ii) an unconventional ChB which can be defined as *orthogonal* ChB (oChB), probably of π-hole nature. At the current state of theoretical studies, we call these weak noncovalent interactions, which are significantly deviated from "angle" IUPAC criterion for chalcogen bonding, as just an induced short contacts involving chalcogen atoms. However, results of QTAIM and NCI analyses reveal that this is favorable and attractive noncovalent interactions. Indeed, appropriate bond critical points were successfully located during QTAIM analysis, attractive nature of these noncovalent interaction additionally was confirmed by $\lambda 2 < 0$ (see blue circles indicated by orange arrows on Figure 7). Also, ELF values in bond critical points for these short contacts involving chalcogen atoms are noticeable, and ELF distribution evidence about the involvement of σ-holes of chalcogen atoms in bonding with oxygen atoms of beta-octamolybdate - we added two appropriate illustrative figures with distribution of ELF in **7** and **8** in Supporting Information (Fig. S12, S13).

In order to compare σ-(Q^{IV})-hole···O=Mo interactions in $\{[Q(bPh)R]_2[Mo_8O_{26}]\}^{2-}$ associates and π-π stacked structural units quantum chemical calculations were performed. The utilized models are shown in Fig. S12-S15. The calculated data describing π-π interactions are summarized in Table S4. The comparison of corresponding energy values shows domination of σ-(Q^{IV})-hole···O=Mo interactions in all the cases. This means that in the isolated complexes, π-π stacking assists crystallization of $\{[Q(bPh)R]_2[Mo_8O_{26}]\}^{2-}$ units but does not induce their formation. Noticeably, **3** and **4** do not show the presence of σ-(Q^{IV})-hole···O=Mo interactions, but feature π-π staking. It looks like in **3** and **4** the $[S(bPh)Mes]^+$ cation with the bulky Mes substituent avoids placing its sulfur atom at too small Δ of 40-50° needed for σ-(S^{IV})-hole···O=Mo NCIs.

View Article Online
DOI: 10.1039/D4QI02258K

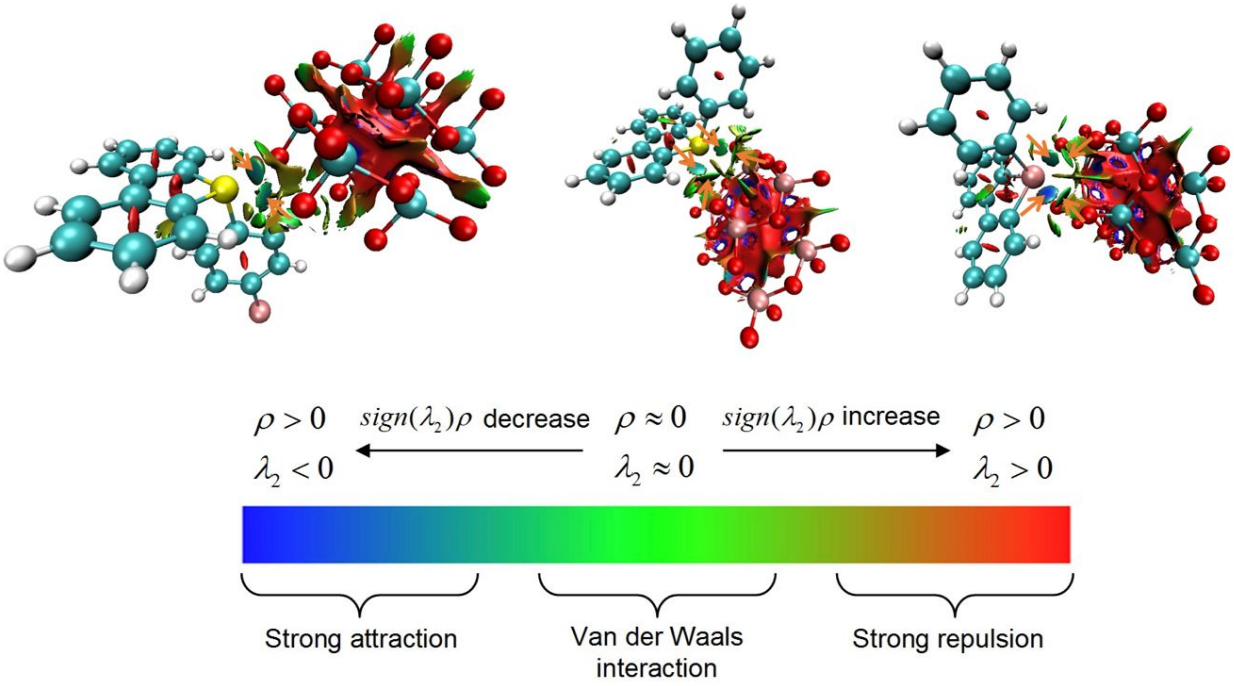

Figure 7. Visualization of NCIs in model supramolecular associates **5**, **7**, and **8** (from left to right; S···O, Se···O, and Te···O contacts indicated by orange arrows) using NCI analysis technique.[87]

Conclusions

Organic-inorganic supramolecular associates consisting of $[Q(bPh)R)]^+$ (Q = S, Se, Te; bPh = $C_{12}H_8$; R = Ph, Mes, 4-BrC_6H_4, 4-FC_6H_4) and beta-octamolybdate anion with various cationic composition can be prepared in a simple way. The nature of cation-anion bonding is cooperative and can be presented as a sum of σ-(Q^{IV})-hole···O=Mo (Q = S, Se, Te) ChB and cation-anion electrostatic interaction. The later component is important but not a unique driving force leading to the formation close associates between the chalconium cations with beta-octamolybdate anion. Depending on the σ-(Q)-hole donor type, the chalconium cation interactions with the $[\beta\text{-}Mo_8O_{26}]^{4-}$ oxobackbone change significantly. Both chalcogen atom and attached organic groups play crucial role in the formation of NCIs. The change of S to Se or Te strongly affects the O…O…Q angle which increases from 40–50° for S to 90° for Te.

These examples unlock the potential of lacunary type polyoxometalates to serve as noncovalent ligands in the comparison with classical heterometal coordination by oxoligands of POM. The existence of vast non-classical coordination chemistry of polyoxometalates based on noncovalent interactions can be anticipated. Chalconium / POM organic-inorganic hybrids demonstrate photochromic behavior firstly reported by Mialane et al.[78] and thoroughly studied by Pradeep et

al.[76,77,89,90] In this regards we demonstrate the association modes between POM and onium cations which is significantly important in the crystal design of such photoactive materials

View Article Online
DOI: 10.1039/D4QI02258K

Acknowledgements:

The NIIC team thanks the Ministry of Science and Higher Education of the Russian Federation for the access SCXRD facilities of NIIC SB RAS. Dmitrii S. Bolotin is grateful to the Saint Peterburg State University for financial support (grant number 103922061). Physicochemical studies were performed at the Center for Magnetic Resonance, Center for X-ray Diffraction Studies, and Center for Chemical Analysis and Materials Research (all at Saint Petersburg State University). Alexander S. Novikov is grateful to the RUDN University Scientific Projects Grant System (project No. 021342-2-000).

References

(1) Breugst, M.; Koenig, J. J. Σ-Hole Interactions in Catalysis. *Eur. J. Org. Chem.* **2020**, *2020* (34), 5473–5487. https://doi.org/10.1002/ejoc.202000660.

(2) Vogel, L.; Wonner, P.; Huber, S. M. Chalcogen Bonding: An Overview. *Angew. Chemie Int. Ed.* **2019**, *58* (7), 1880–1891. https://doi.org/10.1002/anie.201809432.

(3) Kolb, S.; Oliver, G. A.; Werz, D. B. Chemistry Evolves, Terms Evolve, but Phenomena Do Not Evolve: From Chalcogen–Chalcogen Interactions to Chalcogen Bonding. *Angew. Chemie Int. Ed.* **2020**, *59* (50), 22306–22310. https://doi.org/10.1002/anie.202007314.

(4) Lim, J. Y. C.; Beer, P. D. Sigma-Hole Interactions in Anion Recognition. *Chem* **2018**, *4* (4), 731–783. https://doi.org/10.1016/j.chempr.2018.02.022.

(5) Bulfield, D.; Huber, S. M. Halogen Bonding in Organic Synthesis and Organocatalysis. *Chem. – A Eur. J.* **2016**, *22* (41), 14434–14450. https://doi.org/10.1002/chem.201601844.

(6) Heinen, F.; Engelage, E.; Dreger, A.; Weiss, R.; Huber, S. M. Iodine(III) Derivatives as Halogen Bonding Organocatalysts. *Angew. Chemie Int. Ed.* **2018**, *57* (14), 3830–3833. https://doi.org/10.1002/anie.201713012.

(7) Sutar, R. L.; Huber, S. M. Catalysis of Organic Reactions through Halogen Bonding. *ACS Catal.* **2019**, *9* (10), 9622–9639. https://doi.org/10.1021/acscatal.9b02894.

(8) Novikov, A. S.; Bolotin, D. S. Halonium, Chalconium, and Pnictonium Salts as Noncovalent Organocatalysts: A Computational Study on Relative Catalytic Activity. *Org. Biomol. Chem.* **2022**, *20* (38), 7632–7639. https://doi.org/10.1039/D2OB01415G.

(9) Kazi, I.; Guha, S.; Sekar, G. CBr 4 as a Halogen Bond Donor Catalyst for the Selective Activation of Benzaldehydes to Synthesize α,β-Unsaturated Ketones. *Org. Lett.* **2017**, *19* (5), 1244–1247. https://doi.org/10.1021/acs.orglett.7b00348.

(10) Yunusova, S. N.; Bolotin, D. S.; Vovk, M. A.; Tolstoy, P. M.; Kukushkin, V. Y. Tetrabromomethane as an Organic Catalyst: A Kinetic Study of CBr 4 -Catalyzed Schiff Condensation. *Eur. J. Org. Chem.* **2020**, *2020* (43), 6763–6769. https://doi.org/10.1002/ejoc.202001180.

(11) Kniep, F.; Jungbauer, S. H.; Zhang, Q.; Walter, S. M.; Schindler, S.; Schnapperelle, I.; Herdtweck, E.; Huber, S. M. Organocatalysis by Neutral Multidentate Halogen-Bond Donors. *Angew. Chemie Int. Ed.* **2013**, *52* (27), 7028–7032. https://doi.org/10.1002/anie.201301351.

(12) Li, Y.; Ge, Y.; Sun, R.; Yang, X.; Huang, S.; Dong, H.; Liu, Y.; Xue, H.; Ma, X.; Fu, H.; et al. Balancing Activity and Stability in Halogen-Bonding Catalysis: Iodopyridinium-Catalyzed One-Pot Synthesis of 2,3-Dihydropyridinones. *J. Org. Chem.* **2023**, *88* (15), 11069–11082. https://doi.org/10.1021/acs.joc.3c01028.

(13) Wieske, L. H. E.; Erdelyi, M. Halogen Bonds of Halogen(I) Ions─Where Are We and Where to Go? *J. Am. Chem. Soc.* **2024**, *146* (1), 3–18. https://doi.org/10.1021/jacs.3c11449.

(14) Torita, K.; Haraguchi, R.; Morita, Y.; Kemmochi, S.; Komatsu, T.; Fukuzawa, S. Lewis Acid–Base Synergistic Catalysis of Cationic Halogen-Bonding-Donors with Nucleophilic Counter Anions. *Chem. Commun.* **2020**, *56* (67), 9715–9718. https://doi.org/10.1039/D0CC04013D.

(15) Sysoeva, A. A.; Novikov, A. S.; Il'in, M. V.; Suslonov, V. V.; Bolotin, D. S. Predicting the Catalytic Activity of Azolium-Based Halogen Bond Donors: An Experimentally-Verified Theoretical Study. *Org. Biomol. Chem.* **2021**, *19* (35), 7611–7620. https://doi.org/10.1039/D1OB01158H.

(16) Takagi, K.; Murakata, H.; Hasegawa, T. Application of Thiourea/Halogen Bond Donor Cocatalysis in Metal-Free Cationic Polymerization of Isobutyl Vinyl Ether and Styrene Derivatives. *Macromolecules* **2022**, *55* (13), 5756–5765. https://doi.org/10.1021/acs.macromol.2c00281.

(17) Richards, V. Enhanced Enantioselectivity in Halogen-Bonding Catalysis. *Commun. Chem.* **2023**, *6* (1), 140. https://doi.org/10.1038/s42004-023-00940-3.

(18) Pale, P.; Mamane, V. Chalcogen Bonding Catalysis: Tellurium, the Last Frontier? *Chem. – A Eur. J.* **2023**, *29* (69). https://doi.org/10.1002/chem.202302755.

(19) Steinke, T.; Wonner, P.; Gauld, R. M.; Heinrich, S.; Huber, S. M. Catalytic Activation of Imines by Chalcogen Bond Donors in a Povarov [4+2] Cycloaddition Reaction. *Chem. – A Eur. J.* **2022**, *28* (47). https://doi.org/10.1002/chem.202200917.

(20) Portela, S.; Cabrera-Trujillo, J. J.; Fernández, I. Catalysis by Bidentate Iodine(III)-Based Halogen Donors: Surpassing the Activity of Strong Lewis Acids. *J. Org. Chem.* **2021**, *86* (7), 5317–5326. https://doi.org/10.1021/acs.joc.1c00534.

(21) Robidas, R.; Reinhard, D. L.; Legault, C. Y.; Huber, S. M. Iodine(III)-Based Halogen Bond Donors: Properties and Applications. *Chem. Rec.* **2021**, *21* (8), 1912–1927. https://doi.org/10.1002/tcr.202100119.

(22) Heinen, F.; Reinhard, D. L.; Engelage, E.; Huber, S. M. A Bidentate Iodine(III)-Based Halogen-Bond Donor as a Powerful Organocatalyst**. *Angew. Chemie Int. Ed.* **2021**, *60* (10), 5069–5073. https://doi.org/10.1002/anie.202013172.

(23) Mayer, R. J.; Ofial, A. R.; Mayr, H.; Legault, C. Y. Lewis Acidity Scale of Diaryliodonium Ions toward Oxygen, Nitrogen, and Halogen Lewis Bases. *J. Am. Chem. Soc.* **2020**, *142* (11), 5221–5233. https://doi.org/10.1021/jacs.9b12998.

(24) Nishida, Y.; Suzuki, T.; Takagi, Y.; Amma, E.; Tajima, R.; Kuwano, S.; Arai, T. A Hypervalent Cyclic Dibenzoiodolium Salt as a Halogen-Bond-Donor Catalyst for the [4+2]

Cycloaddition of 2-Alkenylindoles. *Chempluschem* **2021**, *86* (5), 741–744. https://doi.org/10.1002/cplu.202100089.

(25) Yunusova, S. N.; Novikov, A. S.; Soldatova, N. S.; Vovk, M. A.; Bolotin, D. S. Iodonium Salts as Efficient Iodine(<scp>iii</Scp>)-Based Noncovalent Organocatalysts for Knorr-Type Reactions. *RSC Adv.* **2021**, *11* (8), 4574–4583. https://doi.org/10.1039/D0RA09640G.

(26) Il'in, M. V.; Polonnikov, D. A.; Novikov, A. S.; Sysoeva, A. A.; Safinskaya, Y. V.; Bolotin, D. S. Influence of Coordination to Silver(I) Centers on the Activity of Heterocyclic Iodonium Salts Serving as Halogen-Bond-Donating Catalysts. *Chempluschem* **2023**, *88* (10). https://doi.org/10.1002/cplu.202300304.

(27) Zhou, B.; Gabbaï, F. P. Anion Chelation via Double Chalcogen Bonding: The Case of a Bis-Telluronium Dication and Its Application in Electrophilic Catalysis via Metal–Chloride Bond Activation. *J. Am. Chem. Soc.* **2021**, *143* (23), 8625–8630. https://doi.org/10.1021/jacs.1c04482.

(28) Weiss, R.; Aubert, E.; Pale, P.; Mamane, V. Chalcogen-Bonding Catalysis with Telluronium Cations. *Angew. Chemie Int. Ed.* **2021**, *60* (35), 19281–19286. https://doi.org/10.1002/anie.202105482.

(29) Tarannam, N.; Voelkel, M. H. H.; Huber, S. M.; Kozuch, S. Chalcogen vs Halogen Bonding Catalysis in a Water-Bridge-Cocatalyzed Nitro-Michael Reaction. *J. Org. Chem.* **2022**, *87* (3), 1661–1668. https://doi.org/10.1021/acs.joc.1c00894.

(30) Wonner, P.; Steinke, T.; Vogel, L.; Huber, S. M. Carbonyl Activation by Selenium- and Tellurium-Based Chalcogen Bonding in a Michael Addition Reaction. *Chem. – A Eur. J.* **2020**, *26* (6), 1258–1262. https://doi.org/10.1002/chem.201905057.

(31) Biot, N.; Bonifazi, D. Chalcogen-Bond Driven Molecular Recognition at Work. *Coord. Chem. Rev.* **2020**, *413*, 213243. https://doi.org/10.1016/j.ccr.2020.213243.

(32) Mahmudov, K. T.; Kopylovich, M. N.; Guedes da Silva, M. F. C.; Pombeiro, A. J. L. Chalcogen Bonding in Synthesis, Catalysis and Design of Materials. *Dalton Trans.* **2017**, *46* (31), 10121–10138. https://doi.org/10.1039/C7DT01685A.

(33) Zhu, H.; Zhou, P.-P.; Wang, Y. Cooperative Chalcogen Bonding Interactions in Confined Sites Activate Aziridines. *Nat. Commun.* **2022**, *13* (1), 3563. https://doi.org/10.1038/s41467-022-31293-5.

(34) Okuno, K.; Nishiyori, R.; Shirakawa, S. Catalysis by Tertiary Chalcogenonium Salts. *Tetrahedron Chem* **2023**, *6*, 100037. https://doi.org/10.1016/j.tchem.2023.100037.

(35) Zhao, C.; Li, Y.; Wang, Y.; Zeng, Y. Cationic Hypervalent Chalcogen Bond Catalysis on the Povarov Reaction: Reactivity and Stereoselectivity. *Chem. – A Eur. J.* **2024**, *30* (24). https://doi.org/10.1002/chem.202400555.

(36) Gleiter, R.; Haberhauer, G.; Werz, D. B.; Rominger, F.; Bleiholder, C. From Noncovalent Chalcogen–Chalcogen Interactions to Supramolecular Aggregates: Experiments and Calculations. *Chem. Rev.* **2018**, *118* (4), 2010–2041. https://doi.org/10.1021/acs.chemrev.7b00449.

(37) Wonner, P.; Vogel, L.; Düser, M.; Gomes, L.; Kniep, F.; Mallick, B.; Werz, D. B.; Huber, S. M. Carbon–Halogen Bond Activation by Selenium-Based Chalcogen Bonding. *Angew. Chemie Int. Ed.* **2017**, *56* (39), 12009–12012. https://doi.org/10.1002/anie.201704816.

(38) Petrov, P. A. Adducts of Sterically Hindered Tellurium Catecholate with Ethers. *Russ. J. Coord. Chem.* **2023**, *49* (6), 357–362. https://doi.org/10.1134/S1070328423600262.

(39) Petrov, P. A.; Filippova, E. A.; Sukhikh, T. S.; Novikov, A. S.; Sokolov, M. N. Sterically Hindered Tellurium(IV) Catecholate as a Lewis Acid. *Inorg. Chem.* **2022**, *61* (24), 9184–9194. https://doi.org/10.1021/acs.inorgchem.2c00751.

(40) Pope, M. T. *Heteropoly and Isopoly Oxometalates*; Springer-Verlag: Berlin, 1983.

(41) Sures, D. J.; Serapian, S. A.; Kozma, K.; Molina, P. I.; Bo, C.; Nyman, M. Electronic and Relativistic Contributions to Ion-Pairing in Polyoxometalate Model Systems. *Phys. Chem. Chem. Phys.* **2017**, *19* (13), 8715–8725. https://doi.org/10.1039/C6CP08454K.

(42) Fullmer, L. B.; Molina, P. I.; Antonio, M. R.; Nyman, M. Contrasting Ion-Association Behaviour of Ta and Nb Polyoxometalates. *Dalton Trans.* **2014**, *43* (41), 15295–15299. https://doi.org/10.1039/c4dt02394c.

(43) Li, Y.-H.; Wang, Z.-Y.; Ma, B.; Xu, H.; Zang, S.-Q.; Mak, T. C. W. Self-Assembly of Thiolate-Protected Silver Coordination Polymers Regulated by POMs. *Nanoscale* **2020**, *12* (20), 10944–10948. https://doi.org/10.1039/D0NR00342E.

(44) Ge, R.; Li, X.-X.; Zheng, S.-T. Recent Advances in Polyoxometalate-Templated High-Nuclear Silver Clusters. *Coord. Chem. Rev.* **2021**, *435*, 213787. https://doi.org/10.1016/j.ccr.2021.213787.

(45) Feng, Y.; Fu, F.; Zeng, L.; Zhao, M.; Xin, X.; Liang, J.; Zhou, M.; Fang, X.; Lv, H.; Yang, G. Atomically Precise Silver Clusters Stabilized by Lacunary Polyoxometalates with Photocatalytic CO 2 Reduction Activity. *Angew. Chemie Int. Ed.* **2024**. https://doi.org/10.1002/anie.202317341.

(46) Shi, J.-Y.; Gupta, R. K.; Deng, Y.-K.; Sun, D.; Wang, Z. Recent Advances in the Asymmetrical Templation Effect of Polyoxometalate in Silver Clusters. *Polyoxometalates* **2022**. https://doi.org/10.26599/POM.2022.9140010.

(47) Wang, J.; Zhou, M.; Yang, D.; Cai, L.; Xiang, S.; Fan, X.; Zhang, J.; Zhang, Z. Integrating Polyoxometalates and Silver Clusters into Atomically Precise Molecular Heterojunction. *Small* **2024**. https://doi.org/10.1002/smll.202404290.

(48) Sun, J.; Abednatanzi, S.; Van Der Voort, P.; Liu, Y.-Y.; Leus, K. POM@MOF Hybrids: Synthesis and Applications. *Catalysts* **2020**, *10* (5), 578. https://doi.org/10.3390/catal10050578.

(49) Zhang, S.; Ou, F.; Ning, S.; Cheng, P. Polyoxometalate-Based Metal–Organic Frameworks for Heterogeneous Catalysis. *Inorg. Chem. Front.* **2021**, *8* (7), 1865–1899. https://doi.org/10.1039/D0QI01407A.

(50) Maru, K.; Kalla, S.; Jangir, R. MOF/POM Hybrids as Catalysts for Organic Transformations. *Dalton Trans.* **2022**, *51* (32), 11952–11986. https://doi.org/10.1039/D2DT01895K.

(51) Luo, X.; Li, F.; Peng, F.; Huang, L.; Lang, X.; Shi, M. Strategies for Perfect Confinement of POM@MOF and Its Applications in Producing Defect-Rich Electrocatalyst. *ACS Appl. Mater. Interfaces* **2021**, *13* (48), 57803–57813. https://doi.org/10.1021/acsami.1c17808.

(52) Miras, H. N.; Vilà-Nadal, L.; Cronin, L. Polyoxometalate Based Open-Frameworks (POM-OFs). *Chem. Soc. Rev.* **2014**, *43* (16), 5679–5699. https://doi.org/10.1039/C4CS00097H.

(53) Sokolov, M. N.; Adonin, S. A.; Abramov, P. A.; Mainichev, D. A.; Zakharchuk, N. F.; Fedin, V. P. Self-Assembly of Polyoxotungstate with Tetrarhodium-Oxo Core: Synthesis, Structure and 183W NMR Studies. *Chem. Commun.* **2012**, *48* (53), 6666. https://doi.org/10.1039/c2cc31692g.

(54) Mukhacheva, A. A.; Shmakova, A. A.; Volchek, V. V.; Romanova, T. E.; Benassi, E.; Gushchin, A. L.; Yanshole, V.; Sheven, D. G.; Kompankov, N. B.; Abramov, P. A.; et al. Reactions of [Ru(NO)Cl 5] 2− with Pseudotrilacunary {XW 9 O 33 } 9− (X = As III , Sb III) Anions. *Dalton Trans.* **2019**, *48* (42), 15989–15999. https://doi.org/10.1039/C9DT03328A.

(55) Chupina, A. V.; Shayapov, V.; Novikov, A. S.; Volchek, V. V.; Benassi, E.; Abramov, P. A.; Sokolov, M. N. [{AgL}2Mo8O26]n– Complexes: A Combined Experimental and Theoretical Study. *Dalton Trans.* **2020**, *49* (5), 1522–1530. https://doi.org/10.1039/C9DT04043A.

(56) Volchek, V. V.; Kompankov, N. B.; Sokolov, M. N.; Abramov, P. A. Proton Affinity in the Chemistry of Beta-Octamolybdate: HPLC-ICP-AES, NMR and Structural Studies. *Molecules* **2022**, *27* (23), 8368. https://doi.org/10.3390/molecules27238368.

(57) Suslonov, V. V.; Soldatova, N. S.; Ivanov, D. M.; Galmés, B.; Frontera, A.; Resnati, G.; Postnikov, P. S.; Kukushkin, V. Y.; Bokach, N. A. Diaryliodonium Tetrachloroplatinates(II): Recognition of a Trifurcated Metal-Involving μ 3 -I···(Cl,Cl,Pt) Halogen Bond. *Cryst. Growth Des.* **2021**, *21* (9), 5360–5372. https://doi.org/10.1021/acs.cgd.1c00654.

(58) Soldatova, N. S.; Suslonov, V. V.; Kissler, T. Y.; Ivanov, D. M.; Novikov, A. S.; Yusubov, M. S.; Postnikov, P. S.; Kukushkin, V. Y. Halogen Bonding Provides Heterooctameric Supramolecular Aggregation of Diaryliodonium Thiocyanate. *Crystals* **2020**, *10* (3), 230.

https://doi.org/10.3390/cryst10030230.

(59) Soldatova, N. S.; Postnikov, P. S.; Suslonov, V. V.; Kissler, T. Y.; Ivanov, D. M.; Yusubov, M. S.; Galmés, B.; Frontera, A.; Kukushkin, V. Y. Diaryliodonium as a Double σ-Hole Donor: The Dichotomy of Thiocyanate Halogen Bonding Provides Divergent Solid State Arylation by Diaryliodonium Cations. *Org. Chem. Front.* **2020**, *7* (16), 2230–2242. https://doi.org/10.1039/D0QO00678E.

(60) Radzhabov, A. D.; Ledneva, A. I.; Soldatova, N. S.; Fedorova, I. I.; Ivanov, D. M.; Ivanov, A. A.; Yusubov, M. S.; Kukushkin, V. Y.; Postnikov, P. S. Halogen Bond-Involving Self-Assembly of Iodonium Carboxylates: Adding a Dimension to Supramolecular Architecture. *Int. J. Mol. Sci.* **2023**, *24* (19), 14642. https://doi.org/10.3390/ijms241914642.

(61) Heinen, F.; Engelage, E.; Cramer, C. J.; Huber, S. M. Hypervalent Iodine(III) Compounds as Biaxial Halogen Bond Donors. *J. Am. Chem. Soc.* **2020**, *142* (19), 8633–8640. https://doi.org/10.1021/jacs.9b13309.

(62) Soldatova, N. S.; Postnikov, P. S.; Ivanov, D. M.; Semyonov, O. V.; Kukurina, O. S.; Guselnikova, O.; Yamauchi, Y.; Wirth, T.; Zhdankin, V. V.; Yusubov, M. S.; et al. Zwitterionic Iodonium Species Afford Halogen Bond-Based Porous Organic Frameworks. *Chem. Sci.* **2022**, *13* (19), 5650–5658. https://doi.org/10.1039/D2SC00892K.

(63) Aliyarova, I. S.; Ivanov, D. M.; Soldatova, N. S.; Novikov, A. S.; Postnikov, P. S.; Yusubov, M. S.; Kukushkin, V. Y. Bifurcated Halogen Bonding Involving Diaryliodonium Cations as Iodine(III)-Based Double-σ-Hole Donors. *Cryst. Growth Des.* **2021**, *21* (2), 1136–1147. https://doi.org/10.1021/acs.cgd.0c01463.

(64) Semenov, A. V.; Baykov, S. V.; Soldatova, N. S.; Geyl, K. K.; Ivanov, D. M.; Frontera, A.; Boyarskiy, V. P.; Postnikov, P. S.; Kukushkin, V. Y. Noncovalent Chelation by Halogen Bonding in the Design of Metal-Containing Arrays: Assembly of Double σ-Hole Donating Halolium with Cu I -Containing O,O-Donors. *Inorg. Chem.* **2023**, *62* (15), 6128–6137. https://doi.org/10.1021/acs.inorgchem.3c00229.

(65) Soldatova, N. S.; Suslonov, V. V.; Ivanov, D. M.; Yusubov, M. S.; Resnati, G.; Postnikov, P. S.; Kukushkin, V. Y. Controlled Halogen-Bond-Involving Assembly of Double-σ-Hole-Donating Diaryliodonium Cations and Ditopic Arene Sulfonates. *Cryst. Growth Des.* **2023**, *23* (1), 413–423. https://doi.org/10.1021/acs.cgd.2c01090.

(66) Yusubov, M. S.; Maskaev, A. V.; Zhdankin, V. V. Iodonium Salts in Organic Synthesis. *Arkivoc* **2011**, *2011* (1), 370–409. https://doi.org/10.3998/ark.5550190.0012.107.

(67) Kumar, S.; Borkar, V.; Mujahid, M.; Nunewar, S.; Kanchupalli, V. Iodonium Ylides: An Emerging and Alternative Carbene Precursor for C–H Functionalizations. *Org. Biomol. Chem.* **2023**, *21* (1), 24–38. https://doi.org/10.1039/D2OB01644C.

DOI: 10.1039/D4QI02258K

(68) Yoshimura, A.; Zhdankin, V. V. Advances in Synthetic Applications of Hypervalent Iodine Compounds. *Chem. Rev.* **2016**, *116* (5), 3328–3435. https://doi.org/10.1021/acs.chemrev.5b00547.

(69) Peng, X.; Rahim, A.; Peng, W.; Jiang, F.; Gu, Z.; Wen, S. Recent Progress in Cyclic Aryliodonium Chemistry: Syntheses and Applications. *Chem. Rev.* **2023**, *123* (4), 1364–1416. https://doi.org/10.1021/acs.chemrev.2c00591.

(70) Takenaga, N.; Kumar, R.; Dohi, T. Heteroaryliodonium(III) Salts as Highly Reactive Electrophiles. *Front. Chem.* **2020**, *8*. https://doi.org/10.3389/fchem.2020.599026.

(71) Soldatova, N. S.; Radzhabov, A. D.; Ivanov, D. M.; Burguera, S.; Frontera, A.; Abramov, P. A.; Postnikov, P. S.; Kukushkin, V. Y. Key-to-Lock Halogen Bond-Based Tetragonal Pyramidal Association of Iodonium Cations with the Lacune Rims of Beta-Octamolybdate. *Chem. Sci.* **2024**. https://doi.org/10.1039/D4SC01695E.

(72) Pantyukhina, V. S.; Volchek, V. V.; Komarov, V. Y.; Korolkov, I. V.; Kokovkin, V. V.; Kompankov, N. B.; Abramov, P. A.; Sokolov, M. N. Tubular Polyoxoanion [(SeMo 6 O 21) 2 (C 2 O 4) 3] 10− and Its Transformations. *New J. Chem.* **2021**, *45* (15), 6745–6752. https://doi.org/10.1039/D1NJ00421B.

(73) Bolle, P.; Albrecht, N.; Amiaud, T.; Humbert, B.; Faulques, E.; Dessapt, R.; Serier-Brault, H. New Robust Luminescent Supramolecular Assemblies Based on [Ln(Mo 8 O 26) 2] 5– (Ln = Eu, Sm) Polyoxometalates. *Inorg. Chem.* **2019**, *58* (24), 16322–16325. https://doi.org/10.1021/acs.inorgchem.9b02941.

(74) Bondi, A. Van Der Waals Volumes and Radii of Metals in Covalent Compounds. *J. Phys. Chem.* **1966**, *70* (9), 3006–3007. https://doi.org/10.1021/j100881a503.

(75) Desiraju, G. R.; Ho, P. S.; Kloo, L.; Legon, A. C.; Marquardt, R.; Metrangolo, P.; Politzer, P.; Resnati, G.; Rissanen, K. Definition of the Halogen Bond (IUPAC Recommendations 2013). *Pure Appl. Chem.* **2013**, *85* (8), 1711–1713. https://doi.org/10.1351/PAC-REC-12-05-10.

(76) Singh, M.; Pradeep, C. P. Modulation of Photocatalytic Properties through Counter-Ion Substitution: Tuning the Bandgaps of Aromatic Sulfonium Octamolybdates for Efficient Photo-Degradation of Rhodamine B. *Dalton Trans.* **2022**, *51* (8), 3122–3136. https://doi.org/10.1039/D1DT03609B.

(77) Kumar, A.; Gupta, A. K.; Devi, M.; Gonsalves, K. E.; Pradeep, C. P. Engineering Multifunctionality in Hybrid Polyoxometalates: Aromatic Sulfonium Octamolybdates as Excellent Photochromic Materials and Self-Separating Catalysts for Epoxidation. *Inorg. Chem.* **2017**, *56* (17), 10325–10336. https://doi.org/10.1021/acs.inorgchem.7b01143.

(78) Hakouk, K.; Oms, O.; Dolbecq, A.; El Moll, H.; Marrot, J.; Evain, M.; Molton, F.; Duboc,

C.; Deniard, P.; Jobic, S.; et al. Sulfonium Polyoxometalates: A New Class of Solid-State Photochromic Hybrid Organic–Inorganic Materials. *Inorg. Chem.* **2013**, *52* (2), 555–557. https://doi.org/10.1021/ic302477p.

(79) Singh, M.; Yadav, A.; Singh, R.; Pradeep, C. P. Aryl Selenonium vs. Aryl Sulfonium Counterions in Polyoxometalate Chemistry: The Impact of Se + Cationic Centers on the Photocatalytic Reduction of Dichromate. *Dalton Trans.* **2024**, *53* (2), 724–737. https://doi.org/10.1039/D3DT03465H.

(80) Beckmann, J.; Dakternieks, D.; Duthie, A.; Ribot, F.; Schürmann, M.; Lewcenko, N. A. New Insights into the Structures of Diorganotellurium Oxides. The First Polymeric Diorganotelluroxane [(p -MeOC 6 H 4) 2 TeO] N. *Organometallics* **2003**, *22* (16), 3257–3261. https://doi.org/10.1021/om021024c.

(81) Bader, R. F. W. A Quantum Theory of Molecular Structure and Its Applications. *Chem. Rev.* **1991**, *91* (5), 893–928. https://doi.org/10.1021/cr00005a013.

(82) Mukhacheva, A. A.; Komarov, V. Y.; Kokovkin, V. V.; Novikov, A. S.; Abramov, P. A.; Sokolov, M. N. Unusual π–π Interactions Directed by the [{(C6H6)Ru}2W8O30(OH)2]6− Hybrid Anion. *CrystEngComm* **2021**, *23* (23), 4125–4135. https://doi.org/10.1039/D1CE00319D.

(83) Abramov, P. A.; Novikov, A. S.; Sokolov, M. N. Interactions of Aromatic Rings in the Crystal Structures of Hybrid Polyoxometalates and Ru Clusters. *CrystEngComm* **2021**, *23* (36), 6409–6417. https://doi.org/10.1039/D1CE00716E.

(84) Mironova, A. D.; Mikhaylov, M. A.; Maksimov, A. M.; Brylev, K. A.; Gushchin, A. L.; Stass, D. V.; Novikov, A. S.; Eltsov, I. V.; Abramov, P. A.; Sokolov, M. N. Phosphorescent Complexes of {Mo 6 I 8 } 4+ and {W 6 I 8 } 4+ with Perfluorinated Aryl Thiolates Featuring Unusual Molecular Structures. *Eur. J. Inorg. Chem.* **2022**, *2022* (7). https://doi.org/10.1002/ejic.202100890.

(85) Popova, V. G.; Kulik, L. V.; Samoilova, R. I.; Stass, D. V.; Kokovkin, V. V.; Glebov, E. M.; Berezin, A. S.; Novikov, A. S.; Garcia, A.; Tuan, H. T.; et al. Noncovalent Dualism in Perylene-Diimide-Based Keggin Anion Complexes: Theoretical and Experimental Studies. *Inorg. Chem.* **2023**, *62* (48), 19677–19689. https://doi.org/10.1021/acs.inorgchem.3c03030.

(86) Espinosa, E.; Alkorta, I.; Elguero, J.; Molins, E. From Weak to Strong Interactions: A Comprehensive Analysis of the Topological and Energetic Properties of the Electron Density Distribution Involving X–H···F–Y Systems. *J. Chem. Phys.* **2002**, *117* (12), 5529–5542. https://doi.org/10.1063/1.1501133.

(87) Johnson, E. R.; Keinan, S.; Mori-Sánchez, P.; Contreras-García, J.; Cohen, A. J.; Yang, W.; Mori-Sánchez, P.; Contreras-García, J.; Cohen, A. J.; Yang, W. Revealing Noncovalent

Interactions. *J. Am. Chem. Soc.* **2010**, *132* (18), 6498–6506. https://doi.org/10.1021/ja100936w.

View Article Online
DOI: 10.1039/D4QI02258K

(88) Contreras-García, J.; Johnson, E. R.; Keinan, S.; Chaudret, R.; Piquemal, J.-P.; Beratan, D. N.; Yang, W. NCIPLOT: A Program for Plotting Noncovalent Interaction Regions. *J. Chem. Theory Comput.* **2011**, *7* (3), 625–632. https://doi.org/10.1021/ct100641a.

(89) Kumar, A.; Devi, M.; Mamidi, N.; Gonsalves, K. E.; Pradeep, C. P. Aromatic Sulfonium Polyoxomolybdates: Solid-State Photochromic Materials with Tunable Properties. *Chem. – A Eur. J.* **2015**, *21* (51), 18557–18562. https://doi.org/10.1002/chem.201503574.

(90) Kumar, A.; Pradeep, C. P. Aromatic Sulfonium Polyoxomolybdates: Tuning the Photochromic Properties through Substitutions on the Counter Ion Moiety. *CrystEngComm* **2018**, *20* (19), 2733–2740. https://doi.org/10.1039/C8CE00345A.

Siberian Branch of Russian Academy of Sciences

Nikolaev Institute of Inorganic Chemistry

3 Lavrentiev Ave., 630090

Novosibirsk, Russia

Tel.: +7-383-316-58-45

e-mail: abramov@niic.nsc.ru

View Article Online
DOI: 10.1039/D4QI02258K

September 6th, 2024

Data Availability Statement

1) CCDC 2381722 (**1**), 2381723 (**2**), 2381724 (**3**), 2381725 (**4**), 2381728 (**5**), 2381727 (**6**), 2381726 (**7**), 2358696 (**8**), 2358690 (**9**), contain the supplementary crystallographic data. These data can be obtained free of charge via http://www.ccdc.cam.ac.uk/conts/retrieving.html, or from the Cambridge Crystallographic Data Centre, 12 Union Road, Cambridge CB2 1EZ, UK; fax: (+44) 1223-336-033; or e-mail: deposit@ccdc.cam.ac.uk.

2) The datasets supporting this article have been uploaded as part of the supplementary information.

Dr. Pavel A. Abramov